Microassembly Fabrication of Tissue Engineering Scaffolds With Customized Design

Han Zhang, *Student Member, IEEE*, Etienne Burdet, *Member, IEEE*, Aun Neow Poo, and Dietmar Werner Hutmacher

***Abstract*—This paper presents a novel technique to fabricate scaffold/cell constructs for tissue engineering by robotic assembly of microscopic building blocks (of volume $0.5 \times 0.5 \times 0.2$ mm^3 and 60 μm thickness). In this way, it becomes possible to build scaffolds with freedom in the design of architecture, surface morphology, and chemistry. Biocompatible microparts with complex 3-D shapes were first designed and mass produced using MEMS techniques. Semi-automatic assembly was then realized using a robotic workstation with four degrees of freedom integrating a dedicated microgripper and two optical microscopes. Coarse movement of the gripper is determined by pattern matching in the microscopes images, while the operator controls fine positioning and accurate insertion of the microparts. Successful microassembly was demonstrated using SU-8 and acrylic resin microparts. Taking advantage of parts distortion and adhesion forces, which dominate at micro-level, the parts cleave together after assembly. In contrast to many current scaffold fabrication techniques, no heat, pressure, electrical effect, or toxic chemical reaction is involved, a critical condition for creating scaffolds with biological agents.**

***Note to Practioners*—Tissue engineering aims at generation of artificial tissues and organs using patient specific cells. Cells obtained from an individual are cultured and seeded onto a 3-D scaffold that will slowly degrade and resorb as the bone structures grow and assimilate *in vivo*. This paper develops a novel robotics technique to fabricate scaffolds with custom properties, which could provide optimal growth conditions. Our technique, consisting of assembling microscopic building blocks, can potentially provide physicians the freedom to design and modify the scaffold surface morphology and topology at the micron level in order to facilitate cellular colonization and organization.**

***Index Terms*—Microassembly, microrobotics, scaffold, tissue engineering (TE).**

I. Introduction

SCAFFOLDS are of great importance for tissue engineering (TE) [1] as they enable the fabrication of functional living implants out of cells obtained from cells culture. Because TE scaffolds will be implanted in the human body, the scaffold materials should be non-antigenic, noncarcinogenic, nontoxic, nonteratogenic, and possess high cell/tissue biocompatibility so as to avoid pathological reactions after implantation. Besides material issues, the macro and microstructural properties of the scaffold are also very important. In general, the scaffolds require individual external shape and well-defined internal structure with interconnected porosity to host cells. From a biological point of view, the designed matrix should [2], [3]:

1) serve as an immobilization site for transplanted cells;
2) form a protective space to prevent unwanted tissue growth into the wound bed and allow healing with differentiated tissue;
3) direct migration or growth of cells via surface properties of the scaffold;
4) direct migration or growth of cells via release of soluble molecules such as growth factors, hormones, and/or cytokines.

A review of techniques to manufacture scaffolds for TE can be found in [4]. Conventional techniques such as solvent casting, fiber bonding, and membrane lamination use toxic solvents which are difficult to remove [5]–[7]. Further, solvent casting and fiber bonding do not allow a multiple layer design, and membrane lamination allows only a limited number of interconnected pore networks. Rapid prototyping technologies such as 3-D printing and 3-D plotting can produce scaffolds with differentiated 3-D structures by joining together liquid, powder, and sheet materials layer by layer according to a computer-generated model. However, this involves thermal treatment or toxic chemicals, so seeding of cells and biological agents can be carried out only after the scaffold has been manufactured. As a consequence, it is difficult to seed cells and nutrients deep into interior regions and to control their distribution.

This paper introduces a novel scaffold fabrication technique which may circumvent major drawbacks of existing techniques by assembling scaffolds from microscopic building blocks which are held together by friction (Fig. 1). This gives flexibility in material selection, pore shape and dimension control, and pore network interconnection. No heat, pressure, electrical reaction or toxic chemical is involved. We envision that each micro building block can be coated and processed to have specific morphology and chemistry and be seeded with specific cells before the assembly, such that distribution can be controlled in 3-D.

To realize this approach requires addressing typical challenges of microrobotics [8] for life science and answering the following questions:

1) Can suitable microparts be formed from biocompatible materials with suitable properties? How can such parts be fabricated in a manner compatible with mass production?

Manuscript received August 30, 2006; revised January 20, 2007, June 9, 2007, August 12, 2007, and September 9, 2007. This paper was recommended for publication by Associate Editor M. Zhang and Editor D. Meldrum upon evaluation of the reviewers' comments. This work was supported by the National University of Singapore.

H. Zhang is with GE Global Research Center, Ltd., Shanghai, China (e-mail: anitazhh@gmail.com).

E. Burdet is with Imperial College London, London SW7 2AZ, U.K. (e-mail: e.burdet@imperial.ac.uk).

A. N. Poo is with the National University of Singapore, 119260 Singapore.

D. W. Hutmacher was with the National University of Singapore, 119260 Singapore. He is now with the Institute of Health and Biomedical Innovation, Queensland University of Technology, Brisbane QLD4059, Australia.

Color versions of one or more of the figures in this paper are available online at http://ieeexplore.ieee.org.

Digital Object Identifier 10.1109/TASE.2008.917011

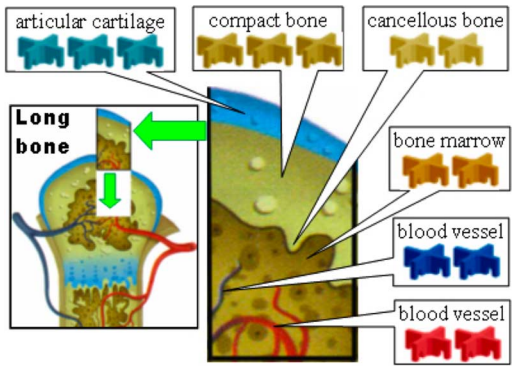

Fig. 1. Fabricating TE scaffolds by assembling microbuilding blocks. Parts can be coated with specific growth factors and cells prior to assembly.

2) Can these microparts be assembled without breaking, in a microassembly task more complex than peg-into-hole [9], [10]?
3) How does one perform or simplify the underlying 3-D manipulation?
4) Will the positioning error grow exponentially with the number of parts? Will the assembly be possible in these conditions?
5) How do material properties and contact forces, dominant at microscopic level, influence the assembly? Is friction sufficient to hold the parts together?

We addressed these questions by combining simulations, design, and a robotic implementation:

1) We examined simple and efficient automatic processes to microassemble scaffolds and designed microparts corresponding to the selected assembly process.
2) We studied whether the forces involved during microassembly are compatible with the targeted materials and investigated how the positioning error grows with an increasing number of microparts and layers.
3) We developed suitable fabrication process for 3-D microparts of 500 μm with wall thickness of 60 μm, provided in a manner to facilitate subsequent coating and assembly.
4) We designed a microgripper to manipulate the microparts, integrated it into a microassembly workstation, and implemented a semiautomatic assembly under visual control.

Different applications of TE require a range of solutions [4]. Here, we target bone reconstruction, i.e., we consider materials with properties corresponding to this application. The presented work demonstrates the feasibility of the microassembly fabrication of scaffold for bone TE, but biological aspects such as cell attachment, as well as a complete automation of the process, will require further work.

Section II presents the concept and feasibility analysis of the microassembly, Section III describes the fabrication of the 3-D microscopic building blocks, and Section IV provides the dedicated workstation for microassembly. Experiments of scaffold assembly are described in Section V. Section VI discusses the system performance and highlights the developed fabrication process.

II. Conceptual Design and Feasibility Analysis

A. Design of Microscopic Building Blocks and Scaffold

Bone TE requires that the scaffold be a template providing special support and that it induces tissue formation. On one hand, the material and structure have to be mechanically strong in order to support existing tissue and the stress of new tissue. On the other hand, material morphology critically influences the formation rate and quality of new tissue [11]–[15]. In this context, assembling microscopic building blocks gives scaffold design flexibility in the following factors:

Surface contour: In bones cites, demineralized bone powder or resorbable calcium phosphates (forming particles between 200–500 μm in diameter) induce new bone to form adjacently; whereas, particles smaller than 125 μm encourage recruitment of macrophage.

Surface roughness: Surface topography influences the rate of bone formation. For instance, rough surfaces enhance synthesis of extracellular matrix and subsequent mineralization; smooth surfaces achieve highest osteocalcin content and alkaline phosphatase activity. Therefore, our technique enables coating with natural polymers and immobilizing growth factors.

Surface chemistry: Incorporation of ions, particles, or chemicals onto the surface can change the orientation of binding proteins and thus change the binding of cells. Part fabrication techniques enables implantation of ions and particles.

Pore aspect ratio and dimension: Pore size affects cell migration, attachment, and proliferation. For example, osteoblasts prefer pore sizes of 200–400 μm [12].

Material: Tissue engineering scaffold material has to be bioresorbable. However, to test the feasibility of the microassembly concept, we can use biocompatible materials with mechanical properties similar to materials used for bone engineering.

B. Design Concept

To simplify the manipulation of the microparts, we decided to assemble scaffolds using only four degrees of freedom motion, in a principle similar to the assembly of Lego parts. Each part is positioned above the previous layer and pushed down vertically into the corresponding parts of this lower layer. The scaffold holds together due to friction and contact forces.

Fig. 2 shows three possible designs of building blocks that can be assembled from above with four degrees-of-freedom (x, y, z, θ_z), where θ_z is the rotation around the z axis. Planar designs [Fig. 2(a)] are simple to fabricate (e.g., using stamping, cutting, or etching) and to grasp but require relatively complicated fixation and positioning. In contrast, 3-D designs [Fig. 2(b) and (c)] are harder to fabricate but can be self-stable, i.e., stand by their own, and require simpler supply and fixation.

We decided to use the 3-D cross shape micropart of Fig. 2(c) for experiments because of the ease of fixation. For bone growth, the suitable pore dimension to accommodate bone cells of about 30–40 μm is 200 to 400 μm [16]. In our case,

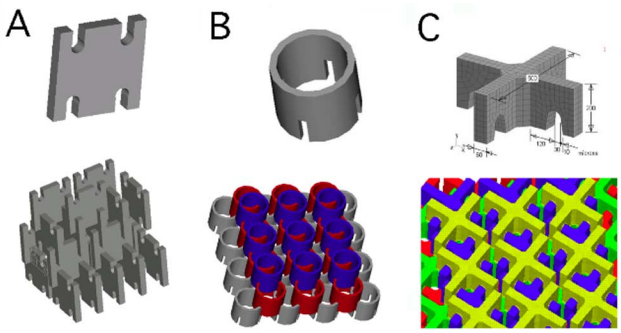

Fig. 2. Lego-like parts can be assembled by pushing them from above using only four degrees-of-freedom. (A) Planar building blocks (of size $0.42 \times 0.42 \times 0.06$ mm). (B) Tubular 3-D microparts. (C) Selected 3-D blocks (of size $0.5 \times 0.5 \times 0.2$ mm with 60 μm wall thickness).

we designed microparts of $500 \times 500 \times 200$ μm in size, 60 μm in wall thickness, which form an interconnected pore network with pore dimension of 280 μm [Fig. 2(c)] and result in about 70% porosity.

C. How Does the Error Grow During Assembly?

In the macro world, it is not difficult, using for example milling or turning techniques, to fabricate parts with 0.1-mm precision, representing a relative error of 0.02% on a typical part of size 0.5 m, which is negligible for most assembly tasks. However, the relative error is much larger in microfabrication. For example, using stereolithography, the typical fabrication error on a 100-μm large part is about 5 μm or 5%. Our microassembly task involves insertion with multiple contact surfaces and will be strongly influenced by the dimensional errors. For instance, when the distance between two walls is much larger than that between the two slots, assembly cannot be achieved.

Position error can also arise from the manipulation system. If the lower two parts are placed too far away or too close, assembly will fail. Our microparts are fabricated by optical lithography with precision of 5 μm and the positioning system has 0.1-μm resolution. The slots of the parts are designed to have 10-μm chamfer (i.e., 10 μm wide and 30 μm high slope on the slots), making the assembly process tolerant to shape errors. However, when more and more parts are fitted, the error might accumulate until it causes a serious problem in assembly. How will the error grow during assembly with an increasing number of microparts and layers? The feasibility of our microassembly concept depends critically on the answer to this question, as for example a scaffold of 1 cm will require approximately 90 layers.

Inside the scaffold, each part is fixed by the lower and upper two parts in which it is in contact. In this way, the part is overconstrained and must be distorted, making it difficult to analyze and determine the position error. In the following, we analyze how error grows with the number of microparts, considering a scaffold with $N \geq 3$ layers, such that all parts are connected together. (With only one or two layers there are several unconnected components and the position error depends on the accuracy of the manipulation.)

To simplify the analysis of error between a part (k_x, k_y) of a given layer and the part at the origin (0,0) in the first layer,

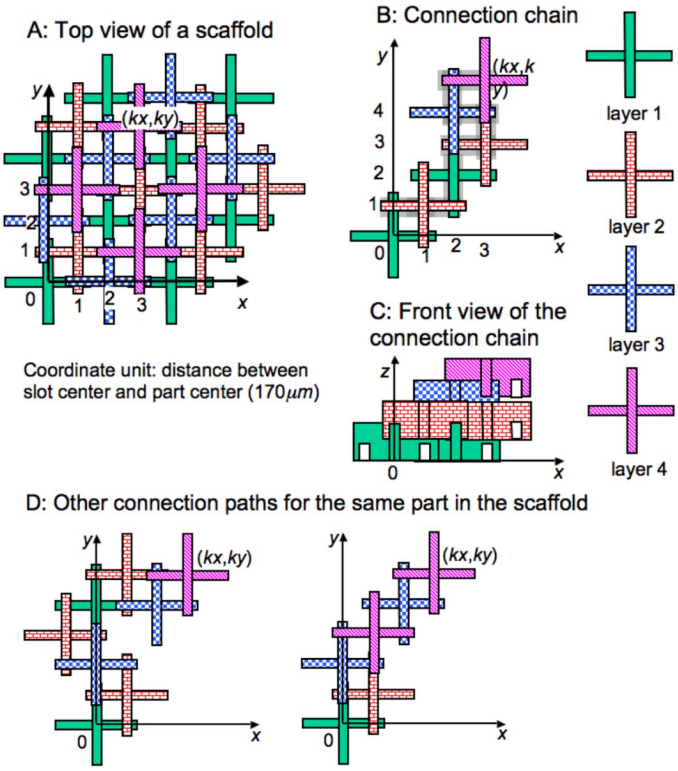

Fig. 3. Stochastic error analysis: Indexes of four consecutive layers in a scaffold with microparts of Fig. 2(c). (B), (C), (D): Part is connected through several parts to the part fixed at origin (0,0). Path shown is (B), (C) and involves a minimal number of parts, and (D) displays another possible path.

we use the shortest, i.e., the most rigid parts chain connecting them and neglected more compliant chains involving more parts (Fig. 3). To further simplify the computations, we consider that the main error source is the distance error from the center of the notch to the center of the part, which we call "shape error" as it is caused by imperfections in the manufacturing process.

We use the following notation: (r_x, r_y) denotes part position at (x, y), and the superscript indicates the layer number. n and p are the distances from slot center to the part center on the negative and positive sides, respectively. They are assumed to be independent normally distributed variables with

$$E[n_x] = E[n_y] = E[p_x] = E[p_y] = 170\ \mu\text{m}$$
$$\sigma[n_x] = \sigma[n_y] = \sigma[p_x] = \sigma[p_y] \equiv \sigma = \frac{5}{3}\ \mu\text{m}. \quad (1)$$

This corresponds to the design in Fig. 2(c), when the manufacturing system is calibrated such that systematic errors are eliminated and other shape errors such as distortion, angle error, etc. are neglected. This simplifies the deviation error analysis without affecting the results. When there are only three layers, we further assume that the parts are rigid. Considering the upper left half of the coordinate plane $(0 \leq k_x \leq k_y)$, we note that $k_x + k_y$ and $k_x - k_y$ are always even (see Fig. 3) and define

$$k_+ \equiv \frac{k_x + k_y}{2}, \quad k_- \equiv \frac{k_y - k_x}{2}. \quad (2)$$

The position of the part (k_x, k_y) is then

$$\begin{aligned} r_x^{(3)}(k_x,k_y) &= \sum_{i=0}^{k_+} n_x^{(2)}(i,i) + \sum_{i=0}^{k_+-1} p_x^{(2)}(i,i) \\ &\quad + -\sum_{i=1}^{k_-} n_x^{(3)}(k_x+i,k_y-i) \\ &\quad - \sum_{i=0}^{k_-} p_x^{(3)}(k_x+i,k_y-i) \\ r_y^{(3)}(k_x,k_y) &= \sum_{i=0}^{k_+} n_y^{(2)}(i,i) + \sum_{i=0}^{k_+-1} p_y^{(2)}(i,i) \\ &\quad + \sum_{i=1}^{k_-} p_y^{(3)}(k_x+i,k_y-i) \\ &\quad + \sum_{i=0}^{k_-} n_y^{(3)}(k_x+i,k_y-i). \end{aligned} \tag{3}$$

As the mean value $E[\cdot]$ is linear, and for normally distributed variables

$$\sigma[x_1+x_2] = \sqrt{\frac{\sigma^2[x_1]+\sigma^2[x_2]}{4}}$$

so $r_x^{(3)}$ and $r_y^{(3)}$ are normally distributed variables with

$$\begin{aligned} E\left[r_x^{(3)}(k_x,k_y)\right] &= 340k_x\ \mu\text{m} \\ \sigma^2\left[r_x^{(3)}(k_x,k_y)\right] &= \frac{50}{9}(k_y+1)\ \mu\text{m}^2 \\ E\left[r_y^{(3)}(k_x,k_y)\right] &= 340(k_y+1)\ \mu\text{m} \\ \sigma^2\left[r_y^{(3)}(k_x,k_y)\right] &= \frac{50}{9}(k_y+1)\ \mu\text{m}^2. \end{aligned} \tag{4}$$

When the fourth layer is assembled, the parts are overconstrained and distortion must happen so that the new part can be fitted in. We further assume that the stiffness of the new part to be placed is much larger than the already assembled parts chains (from the part at origin to the part at destination), and the further a part is from the origin, the more compliant the chain is. In Fig. 3(b), the shadow area shows the force path from part (k_x, k_y) to the origin which is much more compliant than the part itself. Then, we assume that when a part is added in the fourth layer, the two parts in the third layer that are being joined together will produce the same displacement. The position of a part in the fourth layer is thus shown in the equation at the bottom of the page and with mean and variance

$$\begin{aligned} E\left[r_x^{(4)}(k_x,k_y)\right] &= 340(k_x+0.5)\ \mu\text{m} \\ \sigma^2\left[r_x^{(4)}(k_x,k_y)\right] &= \frac{25(k_y+2)}{9}\ \mu\text{m}^2 \\ E\left[r_y^{(4)}(k_x,k_y)\right] &= 340(k_y+1.5)\ \mu\text{m} \\ \sigma^2\left[r_y^{(4)}(k_x,k_y)\right] &= \frac{25(k_y+2)}{9}\ \mu\text{m}^2. \end{aligned} \tag{5}$$

The position error of the fourth layer is smaller than that in the third. After the fourth layer is added, the parts in the third layer will translate due to connection deflection; therefore, the part position becomes

$$\begin{aligned} r_x^{(3)}(k_x,k_y) &= r_x^{(4)}(k_x,k_y) - n_x^{(4)}(k_x,k_y) \\ r_y^{(3)}(k_x,k_y) &= r_y^{(4)}(k_x,k_y) - n_y^{(4)}(k_x,k_y). \end{aligned} \tag{6}$$

Their mean and variance become

$$\begin{aligned} E\left[r_x^{(3)}(k_x,k_y)\right] &= 340k_x\ \mu\text{m} \\ \sigma^2\left[r_x^{(3)}(k_x,k_y)\right] &= \frac{25}{9}(k_y+3)\ \mu\text{m}^2 \\ E\left[r_y^{(3)}(k_x,k_y)\right] &= 340(k_y+1)\ \mu\text{m} \\ \sigma^2\left[r_y^{(3)}(k_x,k_y)\right] &= \frac{25}{9}(k_y+3)\ \mu\text{m}^2. \end{aligned} \tag{7}$$

Compared with (5), we see that the adjunction of the fourth layer reduces the position error in the third layer.

The previous formulation can be extended to the $(2n)$th and $(2n+1)$th layers [19]

$$\begin{aligned} r_x^{(2n)}(k_x,k_y) &= \frac{r_x^{(2n-1)}(k_x+1,k_y+1) + r_x^{(2n-1)}(k_x,k_y)}{2} \\ &\quad + \frac{n_x^{(2n)}(k_x,k_y) - p_x^{(2n)}(k_x,k_y)}{2} \\ r_y^{(2n)}(k_x,k_y) &= \frac{r_y^{(2n-1)}(k_x+1,k_y+1) + r_y^{(2n-1)}(k_x,k_y)}{2} \\ &\quad + \frac{n_y^{(2n)}(k_x,k_y) - p_y^{(2n)}(k_x,k_y)}{2} \\ r_x^{(2n+1)}(k_x,k_y) &= \frac{r_x^{(2n)}(k_x-1,k_y+1) + r_x^{(2n)}(k_x,k_y)}{2} \\ &\quad + \frac{n_x^{(2n+1)}(k_x,k_y) - p_x^{(2n+1)}(k_x,k_y)}{2} \end{aligned}$$

$$\begin{aligned} r_x^{(4)}(k_x,k_y) &= r_x^{(3)}(k_x+1,k_y+1) - p_x^{(4)}(k_x,k_y) - \left[\frac{r_x^{(3)}(k_x+1,k_y+1) - r_x^{(3)}(k_x,k_y)}{2} - \frac{n_x^{(4)}(k_x,k_y) + p_x^{(4)}(k_x,k_y)}{2}\right] \\ &= \frac{r_x^{(3)}(k_x+1,k_y+1) + r_x^{(3)}(k_x,k_y)}{2} + \frac{n_x^{(4)}(k_x,k_y) - p_x^{(4)}(k_x,k_y)}{2} \\ r_y^{(4)}(k_x,k_y) &= r_y^{(3)}(k_x,k_y) + n_y^{(4)}(k_x,k_y) + \left[\frac{r_y^{(3)}(k_x+1,k_y+1) - r_y^{(3)}(k_x,k_y)}{2} - \frac{p_y^{(4)}(k_x,k_y) + n_y^{(4)}(k_x,k_y)}{2}\right] \\ &= \frac{r_y^{(3)}(k_x+1,k_y+1) + r_y^{(3)}(k_x,k_y)}{2} + \frac{n_y^{(4)}(k_x,k_y) - p_y^{(4)}(k_x,k_y)}{2} \end{aligned}$$

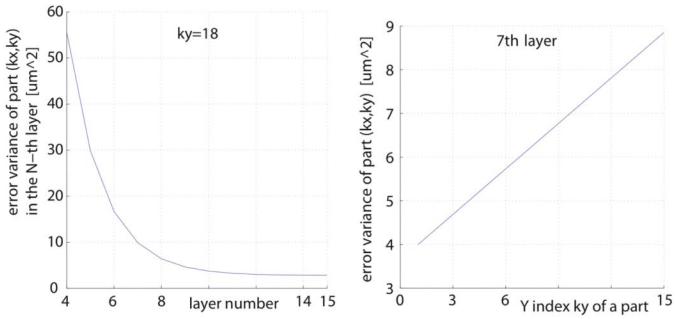

Fig. 4. Stochastic error analysis of how position error of a part located at (k_x, k_y) evolves with an increasing number of parts and layers assembled. (A) Position error decreases with increasing number of layers and becomes similar to shape error. (B) Position error increases linearly with increasing scaffold horizontal dimension. However, the increasing rate is quite lower than that in the perpendicular direction. Position error (σ^2) of a scaffold with 5 mm in horizontal dimension is about 9 μm^2.

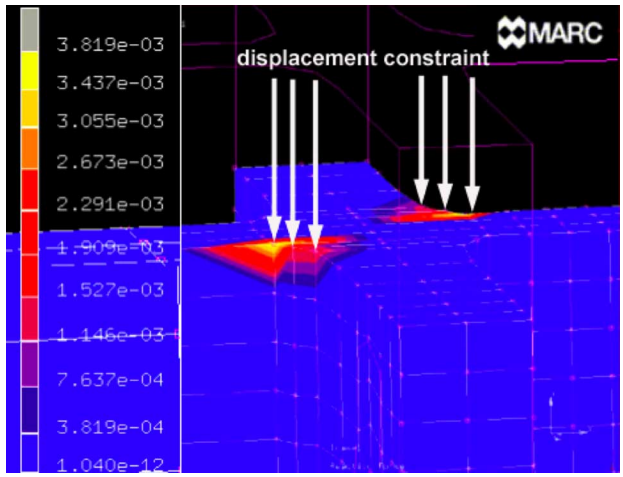

Fig. 5. Local view of reaction force in FEM simulation.

$$r_y^{(2n+1)}(k_x,k_y)=\frac{r_y^{(2n)}(k_x-1,k_y+1)+r_y^{(2n)}(k_x,k_y)}{2}+\frac{n_y^{(2n+1)}(k_x,k_y)-p_y^{(2n+1)}(k_x,k_y)}{2}. \quad (8)$$

The mean and variance for the $(2n)$th layer are [19]

$$E\left[r_x^{(2n)}(k_x,k_y)\right]=340(k_x+0.5)\ \mu\text{m}$$
$$E\left[r_y^{(2n)}(k_x,k_y)\right]=340(k_y+n-0.5)\ \mu\text{m} \quad (9)$$

and for the $(2n+1)$th layer

$$E\left[r_x^{(2n+1)}(k_x,k_y)\right]=340k_x\ \mu\text{m}$$
$$E\left[r_y^{(2n+1)}(k_x,k_y)\right]=340(k_y+n)\ \mu\text{m}. \quad (10)$$

For $N \geq 4$

$$\sigma^2\left[r_x^{(N)}(k_x,k_y)\right]=\sigma^2\left[r_y^{(N)}(k_x,k_y)\right]=\left(\frac{k_y}{2^{N-4}}+\frac{N}{2^{N-3}}+\sum_{i=1}^{N-4}\frac{1}{2^i}\right)\times\sigma^2\ \mu\text{m}^2. \quad (11)$$

The limit for $N \to \infty$ is

$$\lim_{N\to\infty}\sigma^2\left[r_x^{(N)}(k_x,k_y)\right]=\lim_{N\to\infty}\sigma^2\left[r_y^{(N)}(k_x,k_y)\right]=\sigma^2=\frac{25}{9}\ \mu\text{m}^2. \quad (12)$$

This means that in a large scaffold the part position depends only on its own shape error, which is controlled by the manufacturing process.

Fig. 4 shows how the error changes with increasing scaffold size and the number of layers according to the above model. We see that the position variance increases linearly with the size of the scaffold (in the horizontal x-y plane) and decreases with the number of layers. When more than three layers are assembled, each part is overconstrained, which produces internal stress, and part connections must deform to be joined together (Fig. 3). These internal stress and distortions provide an averaging effect reducing the final scaffold dimensional errors, which is similar to elastic averaging designs [17], [18]. Note that no systematic error was assumed in our modeling, though this would not affect the deviation.

Also, due to the internal stress and distortions, the friction at large contact areas between parts contributes to hold them together tightly. The friction is large enough to exceed the weight so that the assembled scaffold can be lifted up by grasping only one part. In our scheme, the parts are assembled from above and push fitted, so the z dimensional error, which grows with scaffold height, can be compensated during the assembly using sensory information.

D. FEM Simulation to Test Assembly Feasibility

The parts should be sufficiently compliant to accept the required deformation in the extreme case of 10-μm misalignment. To investigate whether the parts made of particular biomaterials are likely to break or be damaged during assembly, a 3-D contact simulation using the finite-element method (FEM) was carried out to estimate the involved forces and deformation [19].

Poly ε-caprolactone (PCL), a suitable material for bone engineering, was selected. Its material properties are listed in Table I. Simulation was carried out using MARC [21]. The simulation considers friction proportional to the normal force exerted on the object by the contact surface, i.e., Coulomb friction. It was assumed that the center of the bottom surface of the lower part is fixed. The upper part was placed with 10-μm position error relative to one wall of the lower part, corresponding to an extreme misalignment. The other three branches were neglected to reduce computation to a manageable amount. In the simulation, the upper part moved down until it was fully assembled into the lower part. A 100-μm displacement constraint was exerted on the two edges of the top central area. The results of the simulation suggest the following(Fig. 5):

1) With a maximal misalignment of 10 μm, the microparts will not be crushed by assembly. The maximal stress at the top central area of the upper part is 4 MPa. Thus, with four branches all in extreme misalignment, the stress will be 16 MPa. However, in this simulation, the constraint is added on the two edges. In the real assembly the force is exerted on the top surface so that the stress may be

TABLE I
MECHANICAL PROPERTIES OF POLY(ε-CAPROLACTONE) [20]

polymer	poly(ε-caprolactone)
tensile strength (*MPa*)	16
tensile modulus (*MPa*)	400
Elongation at yield (%)	7.0
Elongation at break (%)	80
Poisson ratio	0.48
friction coefficient	0.2∼0.21

reduced. Further, in compression the material will have higher strength than in tension.

2) Maximal stress at the contact area caused by friction during insertion (at the corner of the straight wall and slope) is about 9 MPa and will not cause any permanent damage.
3) Maximal pressing force is about 4 mN. Thus, with four branches all in 10-μm misalignment, the pressing force can reach 16 mN which will be provided by the gripper. However, we expect a larger force in the real assembly because the tribology is more complex than the simple Coulomb model assumed in our simulation.
4) Since the part weight is only about 0.2 mN, the deformation and contact forces after assembly will help hold the parts together and reduce the final position error.

III. FABRICATION OF BIOCOMPATIBLE BUILDING BLOCKS

Fabricating the microparts of Fig. 2(c) is challenging due to their small size ($0.5 \times 0.5 \times 0.2$ μm overall, 60 μm wall thickness with ± 5 μm tolerance) and complex 3-D shape. Optical lithography or stereolithography can produce microparts from photosensitive biomaterials fulfilling these requirements. Micromoulding techniques such as softlithography and LIGA may be used in the case of nonphotosensitive materials, e.g., PCL [20]. A further requirement is the compatibility of the parts production with the assembly process. A scaffold of one cubic centimeter is composed of about 35 000 parts, so the parts must be produced in a process suitable to mass production and assembly.

We developed the fabrication of SU-8 microparts using optical lithography and plasma etching, which is illustrated in Fig. 6 and described in the following paragraph. The parts are regularly positioned on a wafer and can be easily grasped. SU-8 is a biocompatible material with elasticity modulus of about 4 GPa [22], [23] and mechanical properties similar to poly(L-lactide) (P(L)LA): a very hard biodegradable material which also can be used for bone growth experiments [20]. A second set of microparts was fabricated by IMM-Mainz using an acrylic resin with a rapid micro product development (RMPD) process [24] based on stereolithography. Each layer is 10 μm thick and an accuracy of approximately 5 μm can be achieved in the manufacturing process. The material has a Young's modulus of 349.2 MPa, tensile strength of 14.8 MPa and an elongation at fracture of 5.7%, i.e., mechanical properties similar to PCL.

A silicon wafer was first coated with positive photoresist, patterned under UV light, and developed to have the photoresist covering regions of the notches of the parts. The wafer was then sent for deep reactive ion etching to a depth of 100 μm. After that, there were plateaux on the wafer which were the complement of the notches [Fig. 6(a)]. The photoresist was removed

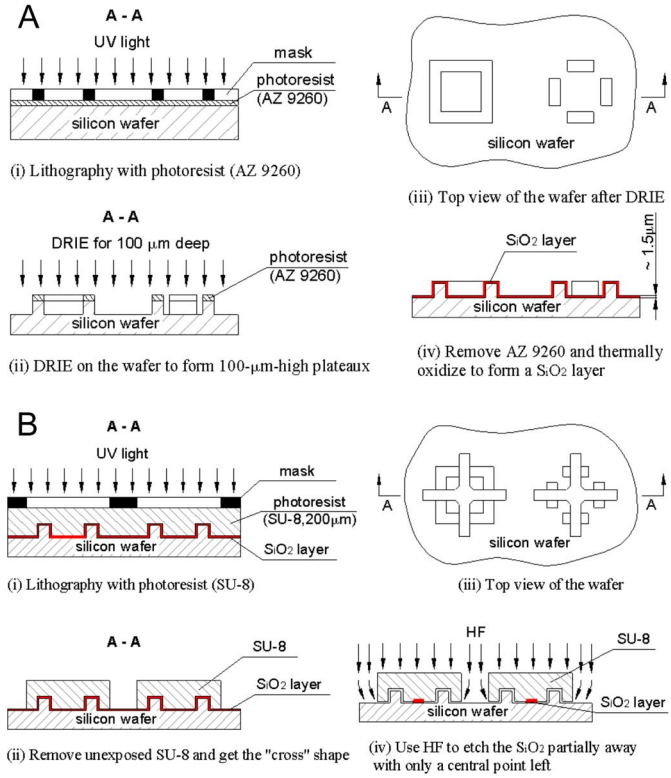

Fig. 6. Fabrication of microparts. (A) Process to create plateaux on a silicon wafer. (B) Created microparts can be easily separated from wafer.

and a sacrificial layer of S_iO_2 was thermally grown. Then, a 200-μm-thick layer of SU-8 was coated on it. Soft baking was then carried out on a hot plate [25]. The hot plate was carefully levelled to be perfectly horizontal so that a flat surface and a uniform layer of equal height across the whole wafer could be obtained as a result of reflow occurring during soft baking. With a good alignment and with the sacrificial layer in between, the SU-8 layer was photopatterned and developed into the cross shapes standing on the plateaux which formed the notches. Finally, the wafer was dipped in hydrofluoric acid (HF) to dissolve the sacrificial oxide layer to separate the microparts from the wafer. HF will etch the oxide layer laterally inwards from the perimeter of the microparts towards the center underneath the part. When the time of HF dipping was set carefully, the cross shape SU-8 part was still fixed on the wafer but with only a small central point connected [Fig. 6(b)]. The detailed process is described in [26]. At the end, the fabricated microparts were regularly disposed on the wafer and could be easily removed from the wafer using a microgripper, which greatly facilitates the scaffold fabrication process (Fig. 7).

IV. WORKSTATION FOR 4DOF MICROASSEMBLY

A. Gripper to Manipulate Biocompatible Microparts

The targeted assembly scheme requires a gripper to grasp the microscopic building blocks with wall size 60 μm, manipulate them without harming the biological agents they bear, bring them to destination in the crowded scaffold environment, and

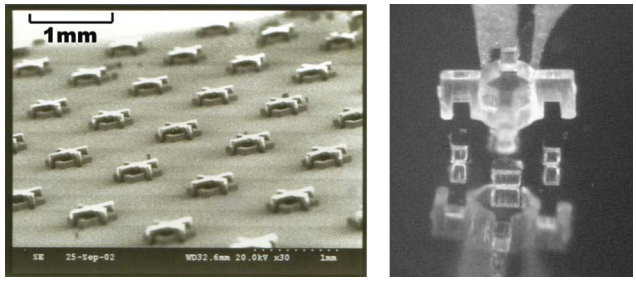

Fig. 7. Microparts fabricated as described in Fig. 6. Microparts are regularly placed on wafer (left) but can be easily detached from it by lifting (right).

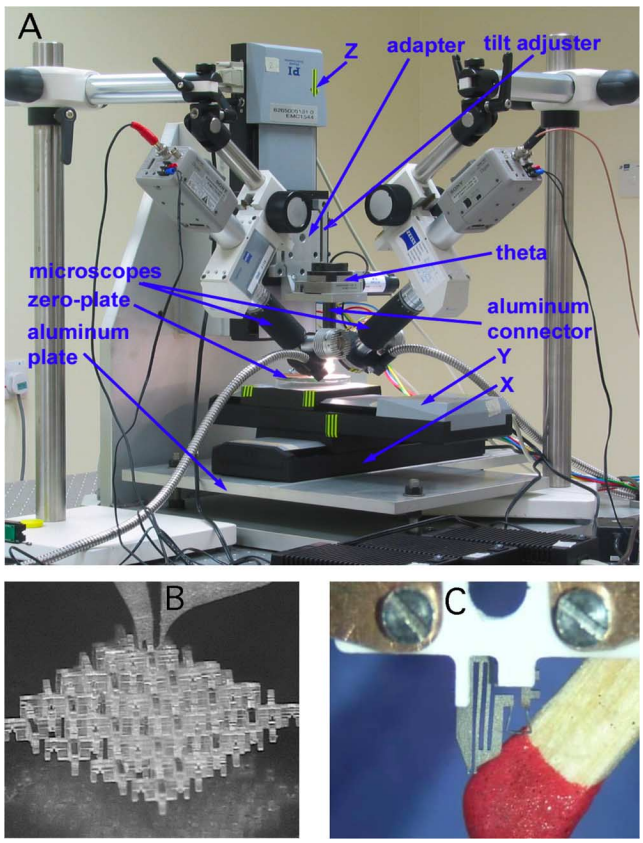

Fig. 8. (A) Dedicated precision workstation for microassembly. (B) Whole scaffold can be lifted up by grasping one part, showing that microparts cleave together without glue or thermal treatment. (C) Shape memory alloy microgripper (compared with a match).

push them with sufficient force in order to fix them on the previous layer. Thus this gripper must be:

1) compact and biocompatible;
2) able to provide sufficient grip force such that a part is not moving relative to the gripper;
3) able to push a part on the previous layer with sufficient force.

A compact gripper with sufficient grasp force was obtained using shape memory alloys [27]. This monolithic microgripper has overall dimension of only 3–4 mm and two fingers of 70-μm width [Fig. 8(c)]. The fixed finger has a plateau on its tip to provide sufficient pressing force for assembly. The other finger's movement is driven by the deformation resulting from the interaction of the actuator and a pullback spring. The actuator has a square shape working as a soft spring with changing stiffness [28]. The pullback spring is a parallel structure which provides pullback force and constrains the finger movement, thus guiding it.

The actuator was locally annealed [29] to induce shape memory effect: it will try to recover its original shape upon temperature-induced phase transformation. However, the remaining parts and in particular the pullback spring remain in the cold-worked state, i.e., no shape memory effect upon temperature changes. An electrical path is integrated to heat the gripper by the Joule effect. A two-step electrical signal is used to drive the gripper. A 0.68 A/0.6 s peak provides fast heat followed by a 0.48-A plateau to maintain the temperature.

After prestraining, the actuator is deformed by the pullback spring. Upon heating, the actuator becomes more rigid, tries to recover its original shape, deforms the pullback spring more, and closes the finger. Upon natural cooling, the actuator softens, is deformed by the pullback spring, thus the gripper opens. The maximal motion range is 80 μm and the grip force is about 30 mN upon 30-μm finger movement. This gripper is capable of manipulating 60-μm-large objects, corresponding to the width of a branch of a micropart Fig. 7(b), right.

The time to cool the gripper is in the order of 1 s, thus a limiting factor of the assembly presented in this paper. Therefore, we have developed a new gripper using adhesion forces as a gripping principle, such that assembly speed is not limited by the physical principle used to grip the parts.

B. Precision Stages and Visual Feedback

Two (PI M-511.DD) translation stages moving in the horizontal $(x\text{-}y)$ plane, fixed together, support the substrate and scaffold [Fig. 8(a)]. The substrate is a silicon wafer etched to have microplateaux which fit the notches of the first layer of the scaffold Fig. 7(b), right. The microgripper is fixed to the rotation stage (PI M-037DG) which is mounted to another translation stage (PI M-511.DDB) moving in the vertical direction (and equipped with a brake so as to lock the stage against falling after power-off). Thus, the microgripper can rotate and move up and down to grasp and assemble the microparts on the assembly table, which is moved vertically relative to it.

An optical linear encoder mounted close to the ballscrew provides a resolution of 0.1 μm for the three translation stages, and the declared accuracy is about 1 μm. The maximal velocity is 50 mm/s and maximal stroke 102 mm. The rotation stage is equipped with precise worm gear drive allowing unlimited rotation in either direction with 0.1° resolution. A (PI C-842) multichannel controller is used to control the four stages.

Two Zeiss (SEC-ZOOM 4) microscopes with a large working distance (of 48 mm) are mounted from the side and provide two images, i.e., 3-D information on the assembly workspace. Two Sony digital cameras with $1/3''$ charge-coupled device (CCD) replace the binocular eyepieces and transmit the grabbed images into the Matrox Meteor II frame grabber and then to the computer.

The $(x\text{-}y\text{-}z\text{-}\theta_z)$ motion actuator and the microscopes are placed on an optical table in a clean room environment [Fig. 8(a)]. The parallelism (θ_z to z), perpendicularity (x-y to z), and coincidence (gripper's rotation axis to θ_z) between axes

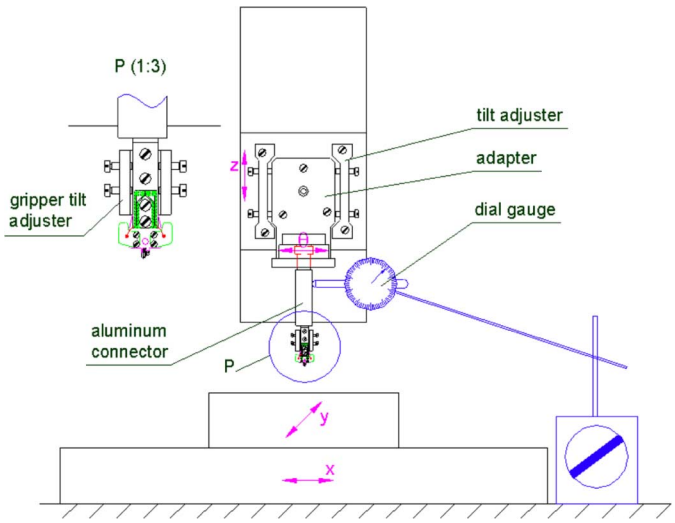

Fig. 9. Robot calibration. Contact surfaces of aluminum connector and adapter are machined with high precision for calibration using a dial gauge.

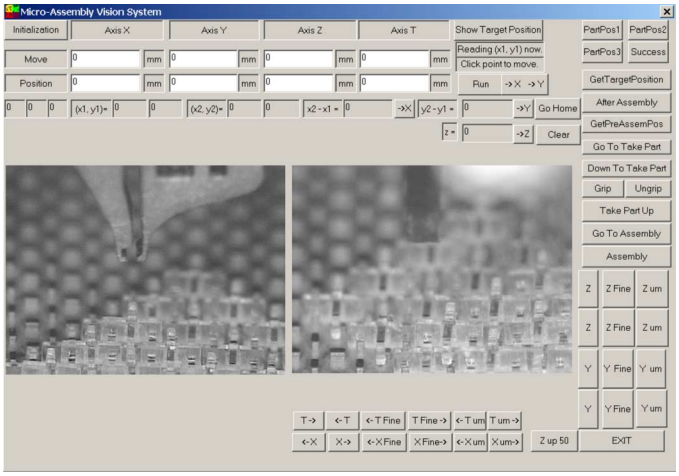

Fig. 10. Control interface.

were calibrated using a dial gauge (Fig. 9) [30]. Fig. 10 shows the graphical user interface. The interface is written in MFC code. The operating system is Windows NT. Communication with control board and ports is achieved by programming through RTX. Matrox Imaging Library (MIL) is used to program the graphics board.

V. Assembly Experiments and Results

A. Semi-Automatic Grasping and Assembly

Microassembly requires micron/submicron position precision and the automation poses challenges for the robotic system [31]–[35]. For a multi-axis robot, an accurate calibration of directionality between axes should be carried out. It will be ideal to have a close-loop control with high-precision position and force feedback [30]. Sensors cannot be easily mounted on the precision mechanism without making them bulky or compromising its functionality. Visual feedback from microscopes is a noncontact alternative to control accurate positioning. The view may be obstructed by the tools or be limited in the crowded environment which is full of fixation mechanisms that are orders of magnitude larger than the parts and micro tools. Additionally, when 3-D visual feedback from microscopes is required, another challenge is how to coordinate the images with limited depth-of-focus. Visual servoing strategies using high magnification optical microscopes and depth-from-focus methods for auto-focus have been investigated in [36] and [37]. These works also investigated the coarse-to-fine visual servoing strategy to realize the transition of visual tracking from wide angle view to fine positioning in micron precision [37].

Since the gripper fingers are very fragile, any scratch or collision between the gripper and the substrate must be prevented. Further, various problems may happen, such as misalignment, tilting, deformation, and distortion. In order to follow the assembly process clearly, it is necessary to adjust the magnification to see a 2×2 mm^2 large area, and the corresponding depth of field is limited to about 400 μm. Therefore, the 100 μm large region in which the assembly takes place and the region where new parts to be assembled are picked up cannot be simultaneously in the field of view of the microscope.

As this paper is focused on proving the feasibility of the assembly concept, tele-operation using a coarse-to-fine motion approach was used to realize safe and relatively fast assembly [8], [36]. During the transport phase, the gripper loaded with the part moves automatically at high speed. When it approaches the destination, the operator takes control and moves it step-by-step, using large 20 μm-long steps and then small 5- and 1-μm-long steps until assembly is completed.

The SU-8 parts are regularly placed on the wafer. The relative position of the scaffold to the parts to be assembled is known, and the gripper automatically finds the position of the part to pick up. The fine approach and grasping is done by the operator. The grasping requires nudging the part slightly to break the joint, after which it can be lifted up and transported.

A correlation computation is then used to identify a suitable target location in the scaffold by searching the desired pattern of the lower two parts on which the new part will be assembled. The substrate holding the lower layers then moves horizontally to the destination, which is at the vertical of the part held by the gripper. Assembly is achieved by the operator by pushing the part down until the notches fit the walls. Then, the gripper releases the assembled part and continues to the next one automatically.

The RMPD microparts from the second set were not disposed regularly on the wafer, so in this case template matching was also used to find a part before picking it (Fig. 11).

B. Release Strategy and Result of Assembly

Releasing the micropart is often problematic as adhesion forces become dominant in the microworld [38]. A releasing strategy was thus developed using the internal stress and adhesion forces maintaining assembled parts together after assembly. The gripper opened and moved 15 μm to let the reference finger leave the part. As the adhesion forces between the gripper and the part decrease rapidly with the distance between the tool and the micro object, the gripper could go up without taking the part with it. Fig. 8(b) shows that after

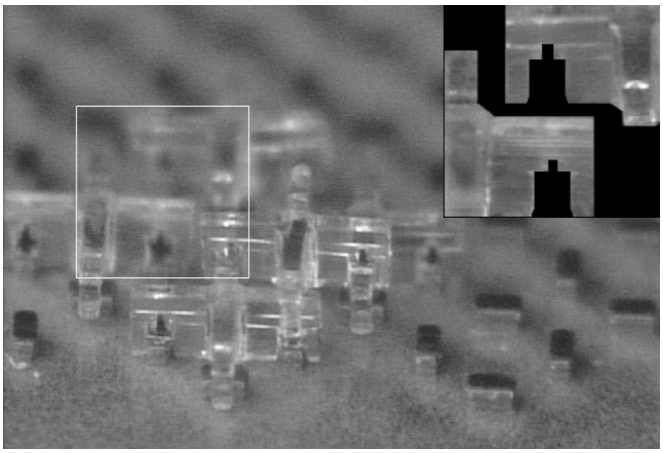

Fig. 11. Determining where to assemble a part using correlation with a sample pattern (shown in right top corner). Algorithm can find a correct position even when image is blurred.

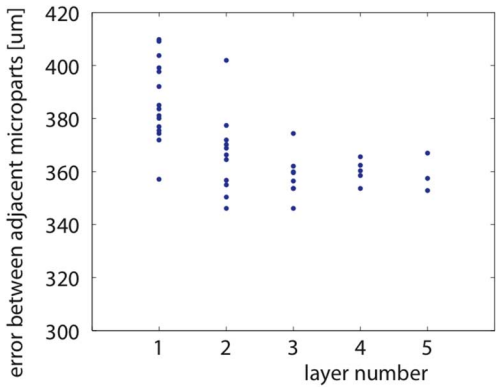

Fig. 12. Implementation confirms that position error decreases when more layers are assembled.

assembly the whole scaffold can be lifted up by grasping a part on the top, demonstrating that friction forces suffice to hold the whole scaffold together. The grasping force of the gripper was measured as described in [27]. When grasping a part, the finger deflection was about 15 μm, which resulted in a grasping force of about 20 mN.

Using the robotic workstation and developed processes, scaffolds were built successfully. The gripper went to the wafer, detached the joint, and lifted the part up without difficulty, then went to the target workspace, decreased the speed when approaching the destination, until assembly was completed. Although positioning errors existed, the parts could be pushed in and assembled together and the positions of the lower two parts were regulated by the above part after assembly. Fig. 8(b) shows a scaffold with seven layers using 50 RMPD parts.

The theoretical error analysis of Section II indicated that the x-y position error of each part will decrease with increasing number of layers. To test this prediction, a seven-layer scaffold was assembled, the bottom of which was not fixed. After each layer was assembled, the distance between each pair of adjacent microparts was measured using a microscope with an x-y stage having 0.5-μm precision to move samples and the variance was computed. This distance is indicative of the position error and determines whether the above part can be assembled or not.

In the scaffold, the first to seventh layers have 16,12, 9, 6, 4, 2, 1 parts, respectively. If a layer contains N parts, then there are $(N-1)$ independent distances in the x-direction and $(N-1)$ in the y-direction. For example, the first layer has in total 30 distances to measure, the second 22, the third layer 16, and so on. The result, shown in Fig. 12, indicates that the error decreased with an increasing number of layers, as was predicted by the stochastic model of Section II. (The top two layers with 2 and 1 parts were not considered.)

VI. Discussion

This paper presented and tested a novel technique to fabricate scaffold/cell constructs for TE. The idea consists of forming 3-D porous structures by assembling biocompatible microscopic building blocks. This concept enables customized design of the scaffold with individual pore morphology, interconnections and scaffold architecture, and controlled concentration of biological signals, cells, and chemicals, by selecting different designs of the microparts and coating them suitably before assembly. In contrast to existing scaffold fabrication techniques, neither heat nor chemicals are involved during the process, and it becomes possible to realize local chemistry and to integrate vascularization.

While these advantages make our fabrication concept attractive to TE, the assembly poses challenges and problems in microfabrication, micromanipulation, fixation, and releasing. A simple assembly principle requiring only four degrees of freedom was proposed in which the microparts are pushed from above like Lego parts.

The first indication of feasibility was provided by a stochastic analysis studying how the error grows with the number of layers. The results suggested that the positioning error of the parts would not increase with the number of layers, indeed it decreases with increasing number of layers and becomes similar to the shape error of a single part. Second, a finite-element simulation of the assembly suggested that parts of biomaterials corresponding to our TE application are sufficiently compliant to be assembled without crushing. The microparts were designed to have 10-μm chamfers to allow positioning error. FEM analysis showed that no plastic deformation happens if the part can be joined (i.e., with maximal misalignment of 10 μm); microassembly will not cause plastic deformation inside the scaffold. After assembly, parts are vertically supported and under compression so that they have much higher yield strength. However, more experiments of large scaffold assembly are required to examine this.

A challenge was to produce microparts with relatively complex 3-D shape using MEMS techniques initially developed for silicon, which had to be adapted to biomaterials. To simplify the fabrication, relatively high tolerance of ± 5 μm was accepted. Although this shape error is high relative to the 60-μm feature dimension, the resulting deformations, together with adhesion forces, should help to connect parts without any adhesive or heat. With the implemented lithography process produced, the microparts are placed regularly on a wafer and can be picked up easily. However, currently the SU-8 parts do not have chamfers

on the notches. Tilting the wafer during DRIE process may form plateaux with slopes and thus form the 10-μm chamfers. Parts produced by stereolithography (built layer after layer) enable 3-D geometry, in particular, to realize notches with chamfers as well as a narrow slot on the notch top to further increase elasticity. The throughput is not as high as optical lithography.

Further testing of this concept is required to implement assembly using appropriate robotics techniques. A microassembly workstation was developed by integrating a microgripper, commercial precision stages, suitable calibration mechanisms, and a semiautomatic control using visual feedback through two optical microscopes. The created shape memory alloy microgripper is suitable for manipulation of biological substrates because heating of the fingers is avoided. It has two fingers driven by a parallel structure which can grasp objects with different shapes and control their orientation, and enables a large pushing force. However, sometimes the part tilted during the insertion. A gripper with more complex shape or a multifinger gripper would enable a more stable grasp.

Manipulation in the microworld is significantly different from the macroworld because capillary, electrostatic, and Van der Waals forces become dominant, which can cause micro-objects to jump to the gripper and prevent their release. Further, fitting microparts together by force is significantly more complex than a simple pick-and-place as it requires controlling the object's orientation, overcoming friction, and resistance from positioning and dimension errors. Instead of attempting to minimize intrinsic forces in the microworld, a successful assembly process was developed by using these forces. In particular, friction, adhesion forces, and material compliance were used to bond the parts and form stable structures.

The realized scaffolds demonstrated the feasibility of this promising concept to build composite scaffolds with complex 3-D shape providing optimal growth conditions and enabling vascularization. The theoretical predictions of the feasibility were verified; in particular, position errors decreased with an increasing number of layers assembled. However, many steps are needed before this technique will be used systematically in TE.

First, the sequential assembly principle is inherently slow, e.g., the pyramid of Fig. 8(b), made of 50 elements, was built in about two hours. With limited improvements we are currently able to pick and place a part every 5 s. An improved automation, the use of parallel grippers and preassembled elements will probably increase the frequency to over 1 Hz. The maximal frequency is not limited by physical principles and will depend on the automation. Second, using several kinds of microparts would bring more flexibility in the possible scaffold architectures and speed up the process. Last but not least, TE requires producing microparts with biodegradable/bioresorbable materials and extensive *in vitro* and *in vivo* testing to examine the cells attachment and proliferation.

ACKNOWLEDGMENT

The authors would like to thank Y. Bellouard, F. Chollet, R. Clavel, A. Shacklock, T. Sidler, and Q. Yang for their contributions to this project.

REFERENCES

[1] R. Langer and J. Vacanti, "Tissue engineering," *Science*, vol. 260, pp. 920–926, 1993.
[2] W. Sun and P. Lal, "Recent development on computer aided tissue engineering: A review," *Computer Methods Programs Biomedicine*, vol. 67, pp. 85–103, 2002.
[3] D. W. Hutmacher, "Polymeric scaffolds in tissue engineering bone and cartilage," *Biomaterials*, vol. 21, pp. 2529–2543, 2000.
[4] H. Zhang, D. W. Hutmacher, F. Chollet, A. N. Poo, and E. Burdet, "Microrobotics and MEMS-based fabrication techniques for scaffold-based tissue engineering," *Macromolecular Biosci. 24*, vol. 5, no. 6, pp. 477–489, 2005.
[5] D. W. Hutmacher, "Scaffold design and fabrication technologies for engineering tissues state of the art and future perspectives," *J. Biomater. Sci. Polymer Edition*, vol. 12, no. 1, pp. 107–124, 2001.
[6] C. M. Agrawal and R. B. Ray, "Biodegradable polymeric scaffolds for musculoskeletal tissue engineering," *J. Biomedical Mater. Res.*, vol. 55, no. 2, pp. 141–150, 2001.
[7] A. G. Mikos and J. S. Temenoff, "Formation of highly porous biodegradable scaffolds for tissue engineering," *Electronic J. Biotechnology*, vol. 3, no. 2, 2000.
[8] D. O. Popa and H. E. Stephanou, "Micro and meso scale robotic assembly," in *Proc. WTEC Workshop: Rev. U.S. Res. Robotics*, 2004, pp. 1–20 [Online]. Available: http://www.wtec.org/robotics/us_workshop/
[9] D. E. Whitney, "Quasi-static assembly of compliantly supported rigid parts," *ASME J. Dynamic Syst., Measurement, Control*, vol. 104, pp. 65–77, 1982.
[10] R. H. Sturges and S. Laowattana, "Virtual wedging in three-dimensional peg insertion tasks," *ASME J. Mechanical Design*, vol. 118, pp. 99–105, 1996.
[11] R. G. Flemming, C. J. Murphy, G. A. Abrams, S. L. Goodman, and P. F. Nealey, "Effects of synthetic micro- and nano-structured surfaces on cell behavior," *Biomaterials*, vol. 20, pp. 573–588, 1999.
[12] B. D. Boyan, T. W. Hummert, D. D. Dean, and Z. Schwartz, "Role of material surfaces in regulating bone and cartilage cell response," *Biomaterials*, vol. 17, pp. 137–146, 1996.
[13] X. F. Walboomers, W. Monaghan, A. S. G. Curtis, and J. A. Jansen, "Attachment of fibroblasts on smooth and microgrooved polystyrene," *J. Biomedical Mater. Res.*, vol. 46, pp. 212–220, 1999.
[14] J. E. Sanders, C. E. Stiles, and C. L. Hayes, "Tissue response to single-polymer fibers of varying diameters: Evaluation of fibrous encapsulation and macrophage density," *J. Biomedical Mater. Res.*, vol. 52, no. 1, pp. 231–237, 2000.
[15] B. Wojciak-Stothard, Z. Madeja, W. Korohoda, A. Curtis, and C. Wilkinson, "Activation of macrophage-like cells by multiple grooved substrata—Topographical control of cell behaviour," *Cell Biology Int.*, vol. 19, no. 6, pp. 485–490, 1995.
[16] K. F. Leong, C. M. Cheah, and C. K. Chua, "Solid freeform fabrication of three-dimensional scaffolds for engineering replacement tissues and organs," *Biomaterials*, vol. 24, pp. 2363–2378, 2003.
[17] A. H. Slocum and A. C. Weber, "Precision passive mechanical alignment of wafers," *J. MEMS*, vol. 12, no. 6, pp. 826–834, 2003.
[18] M. Balasubramaniam, H. Dunn, E. Golaski, S. Son, K. Sriram, and A. Slocum, "An anti backlash two-part shaft with interlocking elastically averaged teeth," *Precision Eng.*, vol. 26, no. 3, pp. 314–330, 2002.
[19] H. Zhang, E. Burdet, D. W. Hutmacher, A. N. Poo, Y. Bellouard, R. Clavel, and T. Sidler, "Robotic micro-assembly of scaffold/cell constructs with a shape memory alloy gripper," in *Proc. IEEE Int. Conf. Robotics and Automation (ICRA)*, 2002, vol. 2, pp. 1483–1488.
[20] L. J. Suggs and A. G. Mikos, "Synthetic biodegradable polymers for medical applications," in *Physical Properties of Polymers Handbook*, J. E. Mark, Ed. Woodbury, NY: Amer. Inst. Physics Press, 1996.
[21] [Online]. Available: http://www.mscsoftware.com/products/marc.cfm
[22] [Online]. Available: http://aveclafaux.freeservers.com/SU-8.html#top
[23] M. O. Heuschkel, M. Fejtl, M. Raggenbass, D. Bertrand, and P. Renaud, "A three-dimensional multi-electrode array for multi-site stimulation and recording in acute brain slices," *J. Neuroscience Methods*, vol. 114, no. 2, pp. 135–148, 2002.
[24] R. Goetzen and A. Reinhardt, "Microstructure and systems production with rapid micro product development (RMPD) for medical and other applications," in *Proc. Int. Conf. Laser Optics for Young Scientists (LOYS)*, 2000.
[25] [Online]. Available: http://www.microchem.com/products/pdf/SU8_50-100.pdf
[26] H. Zhang, F. Chollet, E. Burdet, A. N. Poo, and D. W. Hutmacher, "Fabrication of 3D micro-parts for the assembly of scaffold/cell constructs in tissue engineering," *Int. J. Computational Eng. Sci.*, vol. 4, no. 2, pp. 281–284, 2003.

[27] H. Zhang, Y. Bellouard, E. Burdet, R. Clavel, A. N. Poo, and D. W. Hutmacher, "Shape memory alloy microgripper for robotic microassembly of tissue engineering scaffolds," in *Proc. IEEE Int. Conf. Robotics Automation (ICRA)*, 2004, pp. 4918–4924.
[28] H. Zhang, E. Burdet, D. W. Hutmacher, and A. N. Poo, "Robotic microassembly of scaffolds for tissue engineering," in *Video Proc. IEEE Int. Conf. Robotics Automation (ICRA)*, 2003.
[29] Y. Bellouard, T. Lehnert, J. E. Bidaux, T. Sidler, R. Clavel, and R. Gotthardt, "Local annealing of complex mechanical devices: A new approach for developing monolithic micro-devices," *Mater. Sci. Eng.*, pp. A273–275: 795, 1999.
[30] H. Zhang, "Robotic microassembly of tissue engineering scaffold," Ph.D. dissertation, Nat. Univ. Singapore, 2004.
[31] J. A. Thompson and R. S. Fearing, "Automating microassembly with ortho-tweezers and force sensing," in *Proc. Int. Conf. Robotics and Intelligent Systems (IROS)*, 2001, vol. 3, pp. 1327–1334.
[32] N. Dechev, W. L. Cleghorn, and J. K. Mills, "Microassembly of 3-D microstructures using a compliant, passive microgripper," *J. MEMS*, vol. 13, no. 2, pp. 176–189, 2004.
[33] R. W. Bernstein, X. J. Zhang, S. Zappe, M. Fish, M. Scott, and O. Solgaard, "Characterization of drosophila embryos immobilized by fluidic microassembly," *Transducers*, vol. 2, pp. 987–990, 2003.
[34] Q. Bai, K. D. Wise, and D. J. Anderson, "A high-yield microassembly structure for three-dimensional microelectrode arrays," *IEEE Trans. Biomedical Eng.*, vol. 47, no. 2, pp. 281–289, Feb. 2000.
[35] K. F. Bohringer, K. Goldberg, M. Cohn, R. Howe, and A. Pisano, "Parallel microassembly with electrostatic force fields," in *Proc. IEEE Int. Conf. Robotics Automation (ICRA)*, 1998, vol. 2, pp. 1204–1211.
[36] B. Nelson and B. Vikramaditya, "Visually guided microassembly using optical microscopes and active vision techniques," in *Proc. IEEE Int. Conf. Robotics Automation (ICRA)*, 1997, vol. 4, pp. 3172–3174.
[37] S. Ralis, B. Vikramaditya, and B. J. Nelson, *IEEE Trans. Electronics Packaging Manuf.*, vol. 23, 2000.
[38] R. Fearing, "Survey of sticking effects for micro parts handling," in *Proc. IEEE/RSJ Int. Conf. Intelligent Robots Systems (IROS)*, 1995, vol. 2, pp. 212–217.

Han Zhang (S'02) received the B.S. degree in precision engineering, in 1997, and the M.S. degree in mechanical engineering, in 1999, both from Tsinghua University, Beijing, China, and the Ph.D. degree, in 2004, from the National University of Singapore, where she developed the novel technique described in this paper.

Since 2004, she has worked at GE Global Research, Shanghai, China, on the research and development of MRI devices.

Etienne Burdet (S'92–M'96) received the M.S. degree in mathematics, in 1990, the M.S. degree in physics, in 1991, and the Ph.D. degree in robotics, in 1996, all from ETH-Zurich, Switzerland.

He currently is a Senior Lecturer at Imperial College London, London, U.K. He is doing research at the interface of robotics and bioengineering, and his main research interest is human–machine interaction. He has contributions in various fields from human motor control to VR-based training systems, assistive devices, and microrobotics for life sciences.

Aun Neow Poo received the B.Eng. degree from the National University of Singapore (NUS), in 1968, and the M.Sc. and the Ph.D. degrees from the University of Wisconsin, Madison.

After a year at the IBM Thomas Watson Research Center as a Research Fellow, he joined the NUS as a faculty member in 1974. He was Head of the MPE Department, 1981 to 1992, Dean of Faculty of Engineering, 1983 to 1989, and Director of GSE, 1992 to 1999. His current research interests include mechatronics and intelligent control.

Dr. Poo was a recipient of a Ford Foundation Fellowship.

Dietmar Werner Hutmacher received the B.C. degree from the University for Applied Science, Aachen, Germany, in 1988, and the M.Sc. degree from the University of Utah, in 1988, both in biomedical engineering. He completed his studies with an MBA degree from the Royal Henley Management College, U.K., in 1999, and the Ph.D. degree in tissue engineering from the National University of Singapore, in 2001.

He currently is a Professor and Chair of Regenerative Medicine at Queensland Technical University, Singapore. He is an internationally recognized leader in the field of regenerative medicine, illustrated by his outstanding publication record (more then 110 journal articles, 25 book chapters, and approximately 220 conference papers). He has also edited two books. His publications have collectively been cited more than 1600 times. He is one of the few academics to have taken a holistic bone engineering concept to clinical application. More then 400 patients have been treated with the FDA-approved bone engineering scaffolds developed by a Singapore-based interdisciplinary research group.